Experimental Mechanics
https://doi.org/10.1007/s11340-023-00989-0

RESEARCH PAPER

A Photoacoustic Method to Measure the Young's Modulus of Plant Tissues

O. Zargar[1] · Z. Zhao[2] · Q. Li[3] · J. Zou[2] · M. Pharr[1] · S. Finlayson[3] · A. Muliana[1]

Received: 6 October 2022 / Accepted: 31 July 2023

Abstract

Background The PA method combines optical absorption with acoustic detection of laser-generated ultrasound signals to enable high-resolution and high-speed imaging and determination of the mechanical properties of materials. A measurement of a single point takes only a few seconds; thus, the PA method is high throughput and allows for extracting spatially varying mechanical properties of materials, which is critical in characterizing heterogeneous materials such as biological tissues. As the PA method is non-contact, it precludes damaging the sample surfaces during the measurements.

Objective This study explores the ability of a non-contact and high throughput photoacoustic (PA) method to extract the elastic moduli of bioenergy sorghum tissues, i.e., rind, pith, and vascular bundle, in the axial direction.

Methods A pulsed laser generated a collimated circular beam, which was expanded from 3 mm to 15 mm by a pair of convex lenses. To increase the light absorption, red ink was applied to the sample surface. A focused laser beam from a vibrometer was also delivered at the same location to measure the local surface displacement in the vertical direction. The built-in camera of the vibrometer was used as a monitor.

Results The elastic modulus of the bioenergy sorghum rind was significantly larger than the moduli of the pith and fiber bundles, thus indicating that rind tissues were much stiffer. The statistical results show statistically significant differences among the elastic moduli of the different tissues.

Conclusions These measurements agree well with studies that have implemented other characterization techniques, thus attesting to the utility of the PA technique in characterizing sorghum and other plants going forward.

Keywords Photoacoustic (PA) · Bioenergy Sorghum · Sorghum Tissues · Elastic Moduli

Introduction

It is estimated that agricultural food production will need to increase 70% by 2050 to feed the planet's increasing population, even while facing challenges from climate change and other negative environmental impacts [1]. Stem failure, or stem lodging, is still a major limiting factor in grain production worldwide [2], and its occurrence has increased with more severe and frequent adverse weather events. As stem lodging is a biomechanical problem, mitigation strategies should target the mechano-biological properties of crop stems. One approach to address the stem lodging issue is to breed lodging resistant varieties, which requires a systematic understanding of the interplay between genetics, biomechanical traits of stems, and environments. However, phenotyping of stem biomechanical traits presents a bottleneck. Further complications also arise due to the fact that crop stems are hierarchical structures with different tissue components and direction-dependent mechanical properties (anisotropic behaviors in nature).

Several studies have determined the longitudinal elastic moduli (the moduli along the axial direction) of stems using standard destructive mechanical testing methods, e.g., bending, compression, and tensile tests, that are typically used for engineering materials. Compared to engineering materials, plant stems have irregular shapes and sizes, influencing their responses under standard mechanical testing. To the best of our knowledge, no standardized tests exist specifically for fresh (live) plant tissues, which are complex composite systems often of small size. Moreover, the lack of specific

✉ A. Muliana
amuliana@tamu.edu

[1] Mechanical Engineering Department, Texas A&M University, College Station, TX, USA

[2] Electrical Engineering Department, Texas A&M University, College Station, TX, USA

[3] Soil and Crop Science Department, Texas A&M University, College Station, TX, USA

Published online: 23 August 2023

standards leads to difficulties in extracting useful comparable information from different sources in the literature, particularly for tests on fresh plant stems, which have a high water content [3]. While existing mechanical testing methods are useful for gaining some knowledge of the biomechanical properties of plant stems, improving and standardizing testing and analysis would provide obvious benefits.

Compared to compression and tensile testing, bending tests require minimal sample preparation and can be conducted quickly [4]. The three-point bending test is the most common method used to characterize the mechanical properties of the stem for two reasons: no clamping is required and the test set-up is simple since the sample rests on only two supports while the pointed load is applied to it [5]. A four-point bending test is also recommended as the shear deformation is eliminated at the location of maximum bending moment. Both bending tests cause a stress concentration at the loading region resulting in cross-sectional changes and local crushing. Bending tests have been used to measure the elastic moduli of wood [6, 7], sorghum stems [8–10], wheat stems [11], and maize stems [12]. Tensile tests have also been used to extract the elastic moduli of wood [13], rind strips of maize stems [14, 15], and Arabidopsis stems [16]. Gripping is challenging in this test as clamping a specimen directly to the grip may cause breakage at the grips or slippage issues. Compression tests are also common for woody materials [17], although they cannot be used for thin-walled plant stems as they induce buckling. Moreover, the sample must be short (low length to diameter ratio) and straight enough to avoid sample rotation. Lee et al. [10] utilized uniaxial ramp compression tests with different strain rates on sorghum piths and stems and measured the elastic modulus of the samples. Niklas [18] used bending and twisting experiments to collect the elastic moduli of six herbaceous species with hollow internodes. Al-Zube et al. [4] conducted 3-point bending and compression tests on maize stems and tensile testing on rind strips to measure the elastic moduli of stem internode and constituents. Robertson et al. [12] used 3-point and 4-point bending tests on maize, giant reed, and bamboo to determine the bending modulus and strength of the stems. Gomez et al. [19] used a 3-point bending test on fresh sorghum bioenergy stems to determine the internodes' elastic moduli and flexural stiffness. Recently, Zargar et al. [8] used 4-point bending tests to measure the elastic modulus of sorghum internodes that were mechanically stimulated during growth and development. It was found that periodic bending stimulation during growth of sorghum stems produced internodes with lower elastic moduli.

Several studies have used nanoindentation and atomic force microscopy (AFM) methods to investigate the elastic moduli of tissue components of plant stems, e.g., wood cell walls and plant fibers [20–26]. The nanoindentation method can estimate the surface hardness, - a measure of the resistance to plastic deformation under the applied indentation load- and measure the elastic modulus [5]. AFM has also been used to measure mechanical properties at small scales, e.g., at the level of a single primary cell wall [27, 28]. This method can provide significant information regarding cell wall architecture, e.g., microfibril size and orientation [29–31]. However, both AFM and nanoindentation methods have several disadvantages. The AFM tip radius is around ten nanometers or even smaller, so one of the drawbacks of AFM is that the determination of shape and AFM tip dimensions is difficult [32]. Moreover, the indentation depth compared to the thickness must be small and the sample must be homogeneous and isotropic [33]. To use the nanoindentation method, the sample surface must be extremely flat, which typically requires embedding the sample in resin followed by surface polishing. This sample preparation is challenging and can obscure the properties of the soft tissues. Furthermore, the nanoindentation test is conducted on a small area of plant cell walls and often cannot be used to determine the properties of tissues, comprised of multiple cells. Finally, it is difficult to keep the sample moist after the embedding process. The microindenation method, on the other hand, is suitable for studying the mechanical properties, such as stiffness and turgor pressure, of single cell or multiple cells (tissues) depending on the indenter sizes [33–35]. As with the nanoindentation tests, microindentation testing also requires surface preparation of the samples. Thus, it is desirable to develop a non-contact and higher-throughput method to characterize the mechanical properties of plant tissues.

Recently, high-throughput methods including nondestructive flexural tests, vibrational methods, ultrasound or acoustic methods, and computed tomography (CT) scanning, have also been used to investigate the elastic moduli of plants [36–39]. High-throughput measurements have several advantages that have recently generated considerable interest: reduced costs, high speed of data collection, ease of measurement, capability to test small specimens, and the potential for repeated testing [40]. Nondestructive flexural stiffness experiments can extract information regarding tissue mechanical properties without damaging the specimen and provide good repeatability values [36]. Free vibration and forced vibration methods are the two main dynamic tests for characterizing plant mechanical properties. Free vibration of the plants can be induced by a gust of wind where the plants oscillate at their own natural frequencies. Forced vibration can be induced by striking the plant with a hard object and then measuring the sound waves to calculate the mechanical properties. The free vibration method has been employed to study the biomechanical properties of winter wheat, giant reed, and trees [41, 42]. De Langre et al. [37] have reviewed plant vibration experiments and models applied at different scales. Compared to free vibration, the forced vibration method can determine more than

one frequency simultaneously, increasing the accuracy of the results. Moreover, forced vibration can be conducted on the top flexible part of the plant, where bending tests are usually challenging. Niklas and Moon [43] applied multiple resonant frequency methods to collect the flexural stiffness and modulus of elasticity of *Allium sativum* flower stalks. Zhdanov et al. [39] conducted a dynamic forced vibration method to characterize the elastic moduli of Arabidopsis stems and to assess the effect of turgor pressure on the biomechanical properties of the plant. In addition, several studies have used rapid and non-destructive acoustic/ultrasound testing (stress-wave testing) to measure the flexural modulus of elasticity of wood by calculating the speed of sound through the wood [44–47]. However, this method is challenging for several reasons: the set-up length must be large due to the number of probes required, the structure of wood is complex considering both anisotropic (directional) and inhomogeneous (spatial) variation, and the signal-to-noise ratio (SNR) is low due to the significant wave attenuation on wood. CT scanning can provide beneficial information to evaluate knots in the wood [48–50], detect pith [51], determine fiber orientation [52], evaluate spiral grains [53], and detect wood decay caused by fungi [54, 55]. The field use of CT scanning is challenging, so the samples usually are brought to the CT scanner rather than taking the CT scanner to the field [56]. Recently, Stubbs et al. [38] used CT scan data of maize cross-sections (described in detail in [57]) to model transverse compression loading and extract the elastic moduli of the sample. The method enabled determining the spatial distribution of elastic modulus within the maize cross section from CT scan data intensity.

Table 1 summarizes the elastic moduli of plant stems and tissue components of several crops obtained using standard mechanical testing, including bending, compression, and tensile methods. Most of the data report moduli along the longitudinal axis of the stem, except for a few measurements of the transverse moduli. These limited studies conclude that rind tissues (moduli of 1-50 GPa) are much stiffer than the pith tissues and fiber bundles (moduli of 0.005-3.5 GPa). Table 2 shows the elastic moduli and the stiffness of plant cells (tissues), from microindentation measurements, ranging from 0.1-3 GPa and 2-20 N/m, respectively. Table 3 provides the elastic moduli of plant cell walls of different crops using AFM and nanoindendation methods. Data show that the moduli for the cell walls are above 1 GPa.

The photoacoustic (PA) effect refers to the process of sound or elastic wave formation in light-absorptive materials. When a material is illuminated by light, the thermal expansion caused by the light absorption can form displacements of the target surface and generate bulk acoustic waves, which contain information regarding the optical and mechanical properties of the material. The most significant

Table 1 Standard mechanical testing estimations of the elastic moduli of stem and tissues of different plants

Plant	Elastic Moduli (GPa)	Stem	Pith	Rind	Bundle	Ref
Maize	Compressive Elastic Moduli	10.15 ± 1.47				[4, 57]
	Bending Elastic Moduli	10.06 ± 1.51				[4]
	Tensile Elastic Moduli		0.02-0.19 (Average of 0.14)			[58]
				11.38-35.01 (Average of 19.32)		[4, 14]
	Transverse Elastic Moduli		0.026 ± 0.01	0.85 ± 0.39		[59]
Sorghum	Compressive Elastic Moduli	0.130 ± 0.030	0.036 ± 0.007			[10]
	Bending Elastic Moduli	0.002 – 13.5				[8, 19, 60]
	Tensile Elastic Moduli		0.013 – 0.114	1.4 – 21.1		[61, 62]
Wheat	Compressive Elastic Moduli	0.6 ± 0.11 - 0.9 ± 0.47				[63]
	Bending Elastic Moduli	1.1 ± 0.076 - 2.2 ± 0.23				
	Tensile Elastic Moduli	4.9 ± 0.74 – 13.1 ± 1.5				[63–65]
Barley	Compressive Elastic Moduli	0.42 ± 0.08 - 0.97 ± 0.38				[63]
	Bending Elastic Moduli	1.1 ± 0.063 - 1.4 ± 0.058				
	Tensile Elastic Moduli	4.9 ± 0.74 - 7.3 ± 0.92				
Corn	Compressive Elastic Moduli	3.4 ± 0.57 - 3.5 ± 0.37				
Bamboo	Tensile Elastic Moduli	21.2 ± 11.5			2	[66–69]
Coir		17.3 ± 4.2				[66]
Jute		21.3 ± 12.2 - 24.4 ± 12.0				
Plant tissues	Longitudinal Elastic Moduli		0.005-0.01	24.5-45	0.03-0.84	[70, 71][a]

[a] These are the ranges of elastic moduli of plant tissues

Table 2 Microindentation estimations of the elastic moduli of plant cells

Plant	Elastic Moduli (GPa) / Stiffness (N/m)	Cells	Ref
Tomato	Microindentation test	2.3 ± 0.2 (GPa)	[72]
Onion		2.8 ± 0.2 - 16 ± 1 (N/m)	[73]
Tobacco		0.153 ± 0.043 (GPa)	[35]
	Transverse Elastic Moduli (Microindentation test)	0.591 ± 0.166 (GPa)	
A. thaliana	Microindentation test	12.3-16 (N/m)	[33]

advantages of the PA method are that it is a high throughput and non-contact approach to measure the elasticity of the biomaterial, and it requires minimal sample preparation. The non-contact measurement can eliminate tissue damage, e.g., breaking cell walls, causing water migration, etc., during measurements. Each measurement of a single point takes a few seconds, making the PA method high throughput for measuring spatial properties of tissues. The PA method eliminates the need for extensive surface preparation, such as polishing the tissue specimen, measuring each sample dimension, and placing each sample in the testing fixture; such an extensive sample preparation prior to mechanical testing can disrupt the water content. The PA apparatus is equipped with a laser vibrometer for measuring the axial displacement of the material surface and has an all-optical configuration that does not need physical contact, in contrast to a mechanical method that usually employs an indenter or the ultrasound method that needs a layer of coupling material (water or oil). Because both the probe laser beam of the vibrometer and the excitation laser beam can be highly focused, the test can achieve a lateral resolution of tens or hundreds of microns. Due to these features, the PA effect is widely used for microscopy and material property testing [81–86]. Recently Wang et al. [87] developed a PA phase-resolved method to characterize the biomechanical properties (modulus and viscosity) of tissues using noninvasive viscoelasticity imaging to detect tumor and esophageal disease [88, 89]. To the best of our knowledge, the PA method has not been used previously to characterize the biomechanical properties of plant tissues.

In this study, the PA method was utilized to collect the linear elastic moduli of rind, pith, and fiber bundle tissues of sorghum stems. The optical set-up applied a focused laser beam to illuminate the sample surface and utilized a laser vibrometer to measure the axial displacement of the stem surface. The elastic modulus of the sample can be determined from the waveform of the PA signals. It was hypothesized that the PA method would prove suitable for measuring the elastic moduli of different tissues of sorghum stems and that the results would concur with those obtained using low throughput techniques.

Materials and Methods

Plant Material

Bioenergy sorghum stems were harvested from the field in the summer of 2021 in College Station, Texas (30°33′05.6″N 96°26′14.8″W). Plants were a biomass-type photoperiod sensitive hybrid planted on April 8, 2021. Following emergence the stand was thinned to 65,000 plants ha^{-1}. The plants were grown using standard agronomic practices for local sorghum production, including fertilizers and herbicides. Irrigation was applied as necessary to support robust growth.

Table 3 AFM and nanoindentation estimations of the elastic moduli of plant cell walls

Plant	Elastic Moduli (GPa)	Cell Wall	Ref
Corn	Reduced[a] Elastic Moduli (Nanoindentation test)	Average of 8.86	[74]
Bamboo		14.9 ± 2.1	[23, 66]
Coir		6.0 ± 1.6	[66]
Jute		13.1 ± 1.6 – 14.5 ± 2.5	[66]
Flax fibre		16.9 ± 1.74 - 22.8 ± 1.7	[66, 75, 76]
	Transverse Elastic Moduli (Nanoindentation test)	8	[77]
	AFM test	4.5 ± 0.2 - 21.0 ± 2.9	[75, 77]
Rice	Reduced Elastic Moduli (Nanoindentation test)	19.4	[78]
Cassava		19.0	
Soybean		16.3	
Cotton		16.3	
Wood		8-23	[79]
	Transverse Elastic Moduli (Nanoindentation test)	12.7 – 17.9	[80]

[a] The reduced moduli accounts for moduli of both samples and indenters

Sample Preparation

Plants were harvested for mechanical testing at soil level in the morning before the temperature increased to minimize the loss of tissue water. Stem internode samples were cut into 1 cm sections using a precision saw (Buehler Isomet 1000 Precision saw) to ensure that the top and bottom surfaces of the samples were parallel. To avoid water loss, samples were kept in ziploc bags in a refrigerator before testing. Figure 1 shows the sample cross-section with rind, pith, and vascular bundle tissues. To determine the density of each tissue in the internode, the pith was separated from the rind using steel coring tools, employing a suitable coring diameter based on the overall internode diameter. Vascular bundles were then removed from the pith using small coring tools, followed by forcep-assisted manual extraction of individual bundles. The specimen volume was measured by submerging into a graduated cylinder and measuring the water displacement. The mass of the specimens was measured using a digital balance (model 95364 CEN-TECH ®).

Photoacoustic PA Method

The PA method has been applied to quantify the elasticity of animal tissues [83]. However, most PA elasticity testing approaches use surface waves or bulk waves to extract the elastic properties, which are not feasible for plant tissue testing. Due to the complex inner structure and surface condition of the plant tissue, surface and bulk waves do not readily propagate on the surface or inside the plant tissue. Thus, the vertical displacement of the sample surface during the initial thermal expansion is utilized for the elasticity testing. A pulsed excitation laser beam illuminates a local area to induce thermal expansion, which can be measured by an optical vibrometer. The rise time t_{max} of the vertical displacement is related to elasticity only, which can be estimated by the time difference between the waveform peak and the uprise of the trigger signal. The main frequency of the PA signal is characterized before the test of rising time, and the frequency of the trigger signal is set to be the same as the main frequency. The same trigger signal is applied for both the pulsed laser and the oscilloscope. The elastic modulus can be calculated by [83, 90, 91].

$$E = \frac{3KR^2\rho}{t_{\max}^2} \tag{1}$$

where E is the elastic modulus, R is the radius of the excitation laser spot, ρ is the density of the material, and K is a dimensionless system parameter to be calibrated. The K is ratio of the focal size to the diffraction length and is also used to calibrate the radius of the excitation laser beam [90, 93]. Therefore, the calibration of K should be conducted with the same set-up and conditions as the formal measurement of target materials. The derivation of equation (1) is presented in Appendix A.

Experimental Set-Up

A 532 nm Nd: YAG pulsed laser (Elforlight FQS Series) generated a collimated circular beam, which was expanded from 3 mm to 15 mm by a pair of convex lenses (Lens 1 and Lens 2) and filtered by a pinhole (see Fig. 2). After being reflected by a mirror, the beam was focused by a third lens (Lens 3) on the sample surface. To increase the light absorption, red ink was applied to the sample surface. The diameter of the laser focal spot was approximately 100 μm, the laser pulse energy was 40 μJ, the pulse duration is 4ns, and the pulse repetition rate was set to 40 kHz. A focused laser beam from a vibrometer (Polytec OFV-5000) was also delivered at the same location to measure the local surface displacement in the vertical direction. The built-in camera of the vibrometer was used as a monitor. The diameter of the probe laser beam of the vibrometer was approximately 20 μm. The resolution of the system was determined by the larger laser spot from the excitation laser (≈100 μm). Figure 3 shows an

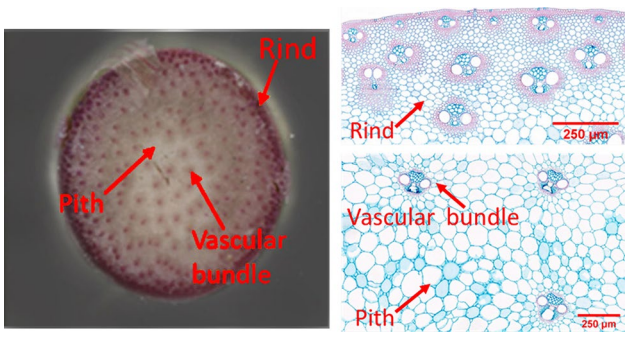

Fig. 1 Cross-section of a stem internode with an average diameter of 19.14 ± 4.47 mm with different tissue components (left) and the close-up images of rind and pith tissues with vascular bundles (right)

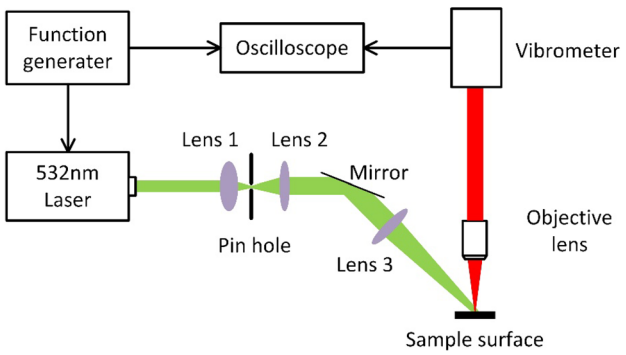

Fig. 2 PA set-up for elasticity test. Lens 1-Lens 3 (Focal length $f_1 = 5$ cm, $f_2 = 25$ cm, $f_3 = 5$ cm)

example of an illuminated sorghum sample during testing. The cross-section of the sorghum showed that the thickness of the rind was about 1 mm, and it also showed the distribution of the pith and vascular bundles relative to the rind (Fig. 1). To obtain the elasticity of the rind, pith, and vascular bundles, 3 random points were measured for each tissue (e.g., the rind) at a distance of 0.5 mm or more away from the boundary between different areas (e.g., the boundary between the rind and pith). The acquisition time for each point was between 2 to 5 seconds. The oscilloscope recorded the waveforms of the signals and the rise time t_{max} was measured. Figure 4(a), (b) and (c) show the waveform from the rind, pith, and vascular bundle. The t_{max} values are 2.86 μs, 5.38 μs, and 15.96 μs for the rind, pith, and vascular bundle, respectively. The blue curves show the original signals, and the orange curves show the triger signals from the function generater. It should be noted that the cell structure of the rind is relatively uniform, so the waveforms are similar to each other, while the waveforms from the pith and vascular bundle may be less homogeneous due to the less uniform cell structure. To estimate the parameter K. Two widely known polymers PET and polycarbonate have been tested, respectively. The densities of the PET and polycarbonate are 1350 kg/m^3 and 1200 kg/m^3. The Young's moduli are 3550 MPa and 2000 MPa. The rise times t_{max} are acquired as 2.53 μs and 3.23 μs for PET and polycarbonate, respectively. Based on equation (1), the K value from the PET and polycarbonate are 249±11 and 259±7, respectively. Based on the data from the PA signals of PET and polycarbonate, the K value used in this paper is 254.

Data Analysis

Data was acquired through the oscilloscope and processed in MATLAB® R2021b version 9.11. Statistical analysis was performed using R (version 4.1.1) and RStudio (version 1.4.1717). Two-way analysis of variance (ANOVA) was used to identify differences in densities and elastic moduli of tissues, with the significance level at $\alpha_{SL} \leq 0.05$.

Results

The density and elastic moduli of the tissues, e.g., rind, pith, and bundles, are summarized in Figs. 5 and 6, respectively. The data were collected from different internodes (internodes 3-9) in the stems and obtained from different stems (8-10 stems). Tables 1A, 2A, 3A, 4A in Appendix B show the statistical results from the ANOVA for density and elastic modulus. The main effect of tissue was significant without interaction for both density and elastic modulus, which means the density and elastic modulus varied depending on tissue types. Multiple comparisons were also conducted to further investigate differences among the three tissues. The statistical results show that the density difference between pith and bundles was not significant; however, the density of pith and bundles was significantly different from the density of the rind. The statistical results also show statistically significant differences among the elastic moduli of the different tissues. The elastic moduli of both pith and bundle tissues were smaller (in the range of 0.15-1.6 GPa) than the modulus of the rind tissue (in the range of 3.9-10 GPa).

Discussion

A PA method was used to determine the elastic moduli of different tissues, i.e., rind, pith, and vascular bundles of mature bioenergy sorghum internodes. The PA method is a non-contact high throughput technique to determine local mechanical properties of tissues based on optical wave propagation, i.e., a coupling of light absorption and

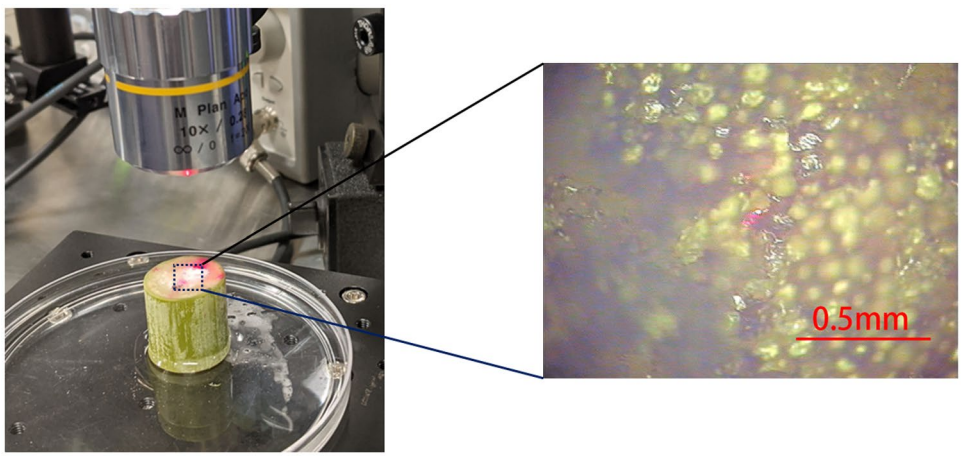

Fig. 3 The target tissue is illuminated by a short laser pulse

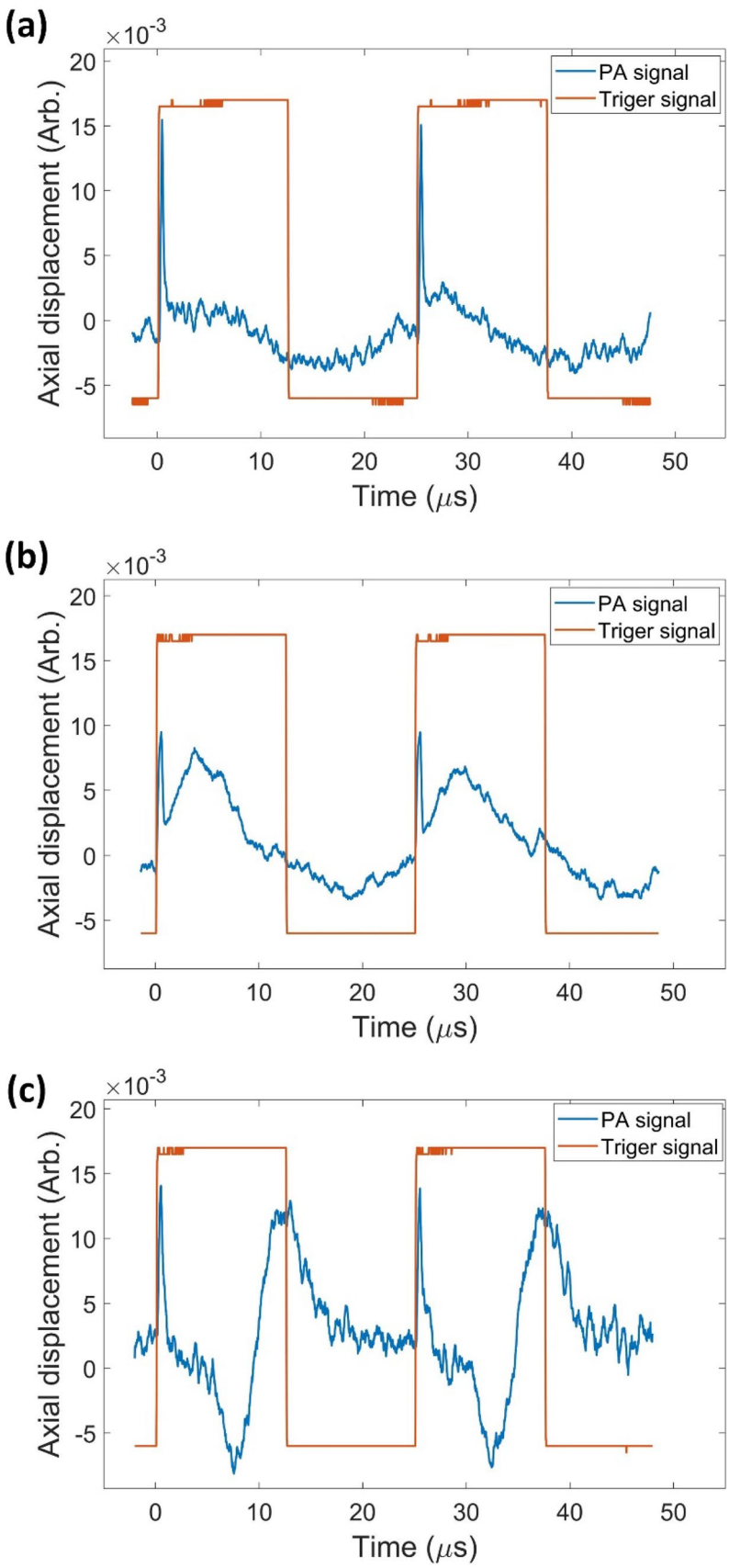

Fig. 4 PA signals from the rind, pith, and vascular bundle

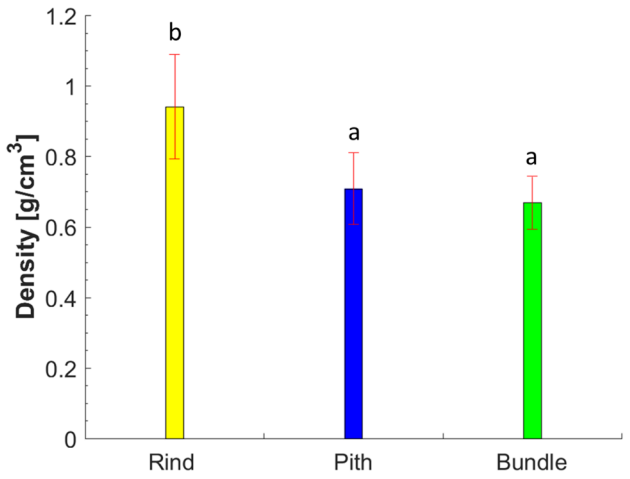

Fig. 5 Density comparison between the stem constituents (rind, pith, and bundle) of internodes 3 to 9. The data are means ± Standard Error (SE). Different letters indicate statistically significant differences ($P < 0.05$; F-test, please refer to Table 2B)

displacement. In this study, the PA method was used to determine the elastic moduli of the tissues along the longitudinal (axial) direction of the stems.

The density of different tissues was first characterized. The statistical results show that the density difference between the pith and vascular bundles was not significant; however, the density difference between these tissues and the rind was statistically significant (0.9412 g/cm^3 for rind, 0.7086 g/cm^3 for pith, and 0.6685 gr/cm^3 for bundle in average). Among all the tested tissues, the rind had the highest density. This larger density might be because the rind tissue has smaller, more tightly packed cells than the pith tissue, while the vascular bundle has a variation in the size of its cells (see Fig. 1).

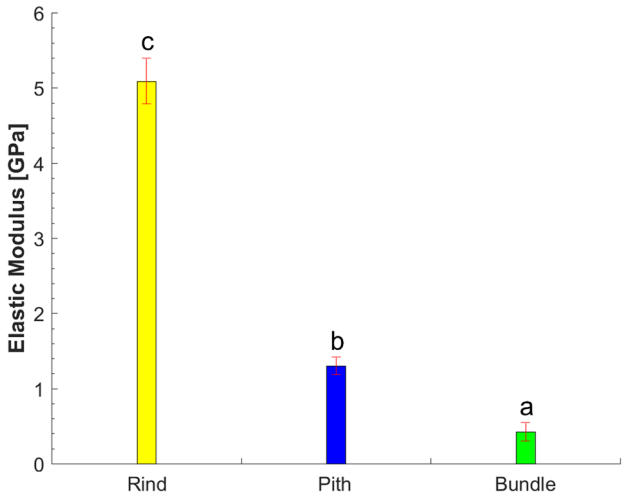

Fig. 6 Elastic moduli comparison between the stem constituents (rind, pith and bundle) of internodes 3 to 9. The data are means ± SE. Different letters indicate statistically significant differences ($P < 0.05$; F-test, please refer to Table 4B)

The elastic modulus of the rind determined from the PA method was in the range of 3.9-10 GPa (6.7 GPa on average), which is quite consistent with the values determined by conventional mechanical testing methods (uniaxial tests) shown in Table 1, and in particular with the values from tensile testing data for Della sorghum in the range of 3-9 GPa [62]. In general, the elastic modulus of sorghum rind from tensile tests has been reported in the range of 1.4-21.1 GPa and for maize, tensile tests have provided estimates in the range of 11-35 GPa. The pith and vascular bundle moduli from the PA method were in the range of 0.15-1.6 GPa (0.85 GPa and 0.59 GPa on average, respectively). By comparison, the elastic modulus of sorghum pith based on Table 1 is 0.013-0.114 GPa with uniaxial tests. The discrepancy between our data with Table 1 most likely arises from the genotype difference, as Table 1 refers to Della sorghum while herein we use bioenergy sorghum hybrids. Furthermore, Table 1 sorghum pith data was derived from greenhouse grown plants, while the data presented here is based on field grown plants. Field grown plants have higher elastic moduli compared to greenhouse plants due to environmental effects. Reference [91] shows that the tissue stiffness of the parenchyma for *Arundo donax* is in the range of 0.4-1 GPa although it has not been reported for sorghum.

The PA method also indicated that the rind tissues were much stiffer than the pith and vascular bundle, consistent with reports from the literature. The elastic modulus of the bundle was lower than that of the pith (0.59 GPa vs. 0.85 GPa). To the best of our knowledge no prior data comparing the mechanical properties of pith vs. vascular bundles exists for sorghum. However, data does exist in similar plants (e.g., maize, rice), which indicated the vascular bundles were stiffer than pith tissues. In one study [38] for dry maize stems the authors showed that the softest tissue was pith and the stiffest tissue was rind, while the stiffness of vascular bundles was somewhere between the pith and the rind. Another study for wet rice stems [92] showed that the vascular bundle elastic modulus was much larger than pith tissues (7.17 GPa vs. 0.44 GPa). The variations in the elastic moduli of the different tissues may be attributed to their differing cell wall thicknesses, composition, and organization.

The PA method is a non-contact and high-throughput method. Compared with other mechanical testing methods such as microindentation, nanoindentation, and AFM, the PA stands out as it avoids damaging the tissue such as breaking cell walls and causing water migration during the measurements. The PA approach is fast, allowing the measurement of every single location (tissue) to be completed with a single pulse (pulse duration 4 ns).

Future studies can consider the measurement of anisotropic moduli of the different tissues of plant stems, which

requires cutting specimens in different directions. The PA method is also suitable for determining the viscosity of the tissues, which will be considered for future studies. Additionally, in principle, the PA approach can facilitate 2D mapping of the spatial distribution of the elastic modulus. However, this ability requires the surface to be nearly flat for uniform laser illumination of different locations. Hence, 2D mapping using PA method can be included in future studies.

Conclusions

To examine the elastic moduli of different tissues, i.e., rind, pith, and vascular bundle of bioenergy sorghum internodes, a non-contact and high throughput PA method was implemented. The rind tissue had the highest modulus, while the vascular bundle had the lowest modulus, indicating that the rind tissues were much stiffer than the pith and vascular bundle. The measured elastic moduli of these tissues along the axial direction of the stems appeared to be consistent with the moduli of sorghum determined using conventional mechanical testing methods. This consistency suggests that the PA method is reliable for obtaining the elastic moduli of the different tissues within the stem internodes. Compared with other local mechanical measurement methods, such as microindentation, nanoindentation, and AFM, the PA method has the advantage of being high-throughput and requires less sample preparation, which minimizes the chance of modifying the tissue properties during sample preparation and measurement.

Appendix A

This Appendix presents the derivation of equation (1) [90, 93], which was used to determine the elastic modulus of the tissues from PA signals**.** The PA method is based on solving a wave propagation equation of motion $\frac{d\tau_z}{dr} + F_z = \rho\frac{\partial^2 u_z}{\partial t^2}$ in a linear viscoelastic material under shear deformations with the following linear viscoelastic model $\tau_z = G\gamma_z + \mu\frac{d\gamma_z}{dt}$, where τ_z is the shear stress and the shear strain is given as $\gamma_z = \frac{du_z}{dr}$ and G and μ are the shear elastic modulus and viscosity, respectively . The wave propagation equation of motion is then written by $G\frac{d^2u_z}{dr^2} + \mu\frac{d}{dt}\left(\frac{d^2u_z}{dr^2}\right) + F_z = \rho\frac{\partial^2 u_z}{\partial t^2}$ and with an algebraic manipulation we have:

$$\frac{\partial^2 u_z}{\partial t^2} - \left(C_T^2 + \eta\frac{\partial}{\partial t}\right)\Delta_\perp u_z = F_z \tag{A.1}$$

where u_z is the displacement, z is the incident direction of the laser, C_T is the shear wave velocity, $\Delta_\perp$ is the 2D Laplacian operator, $\eta = \frac{\mu}{\rho}$ is the kinematic viscosity which depends on the viscosity μ and the density ρ, and F_z is the equivalent excitation laser force. In the laser-illuminated area with a radius near 50μm, the plant tissue is assumed to be elastically isotropic [83]. The relation between the wave velocity and the shear modulus G is written as:

$$C_T = \sqrt{\frac{G}{\rho}} \tag{A.2}$$

The Young's modulus and shear modulus are related by Poisson's ratio υ:

$$G = \frac{E}{2(1+\upsilon)} \tag{A.3}$$

The plant tissue is generally assumed to be incompressible with a Point ratio υ near 0.5. The shear modulus can be further estimated as:

$$G \approx \frac{E}{3} \tag{A.4}$$

Substituting equation (A.4) into equation (A.2); the shear velocity C_T can be estimated as:

$$C_T \approx \sqrt{\frac{E}{3\rho}} \tag{A.5}$$

For a pulsed Gaussian laser beam, the equivalent excitation force can be given by:

$$F_Z = \alpha\Gamma I_0 f(t)\exp\left(-\alpha z - \frac{r^2}{R^2}\right) \tag{A.6}$$

where α is the light absorption coefficient, Γ is the Gruneisen parameter, I_0 is the initial laser intensity, $f(t)$ is the delta function which is used to represent the laser pulse, r is the radial coordinate, and R is the waist radius of the Gaussian laser beam. Because the laser pulse duration can usually be short with a magnitude order of ns, the heat conduction has been neglected. The Substituting equations (A.5), (A.6) into equation (A.1), the PA-generated shear wave equation can be rewritten as:

$$\frac{\partial^2 u_z}{\partial t^2} - \left(C_T^2 + \eta\frac{\partial}{\partial t}\right)\Delta_\perp u_z = \alpha\Gamma I_0 f(t)\exp\left(-\alpha z - \frac{r^2}{R^2}\right) \tag{A.7}$$

To analytically solve the vertical displacement at the center of the laser beam, a Hankel transform is conducted on both sides of equation (A.7) which was discussed in in [90, 93]. By considering a Gaussian laser and delta function pulse, the displacement at the center of the laser beam is given by:

$$u_z = \frac{\alpha\Gamma I_0 R\delta}{\rho C_T}\frac{\frac{\sqrt{E/3\rho}}{R}t}{1 + \frac{4\mu}{\rho R^2}t + \left(\frac{\sqrt{E/3\rho}}{R}t\right)^2} \tag{A.8}$$

where δ is the laser pulse width. By differentiating u_z on t, the displacement u_z reaches its peak at t_{max}:

$$t_{max} = \frac{R}{\sqrt{E/3\rho}} \tag{A.9}$$

The estimation of Young's modulus from the PA method can be affected by the size of the laser beam [90, 93]. To account for the size effect, a parameter K, which is ratio of the focal size to the diffraction length, needs to be first calibrated:

$$E = \frac{3KR^2\rho}{t_{max}^2} \tag{A.10}$$

Appendix B

This Appendix presents the statistical results for density and elastic moduli comparison of the tissues.

Table 1B Two-way ANOVA table of tissue densities. The tissue factor contains three levels: rind, pith, and bundle, while the internode factor contains 7 levels: IN3-9

Two-way ANOVA-Density				
	df	**Sum of squares**	**F value**	***p* value**
Internode	6	3.1131	3.2235	**0.0051**
Tissue	2	3.3004	10.2522	**< 0.0001**
Internode:Tissue	12	1.3977	0.7236	0.7270
Residuals	165	26.5584		

Table 2B Multiple comparisons of tissue densities

Tissue	**emmean**[a]	**SE**	**df**	**lower.CL**	**upper.CL**	**Group**
Bundle	0.6981	0.0524	165	0.5946	0.8016	**a**
Pith	0.7596	0.0524	165	0.6561	0.8631	**a**
Rind	1.0325	0.0524	165	0.9290	1.1360	**b**

[a]estimated marginal mean

Table 3B Two-way ANOVA table of tissue elastic moduli. The tissue factor contains three levels: rind, pith, and bundle, while the internode factor contains 7 levels: IN3-9. Square root transformation was applied to the modulus

Two-way ANOVA-Modulus				
	df	**Sum of squares**	**F value**	***p* value**
Internode	6	2.052	1.5602	**0.1621**
Tissue	2	90.008	205.296	**< 0.0001**
Internode:Tissue	12	1.086	0.4128	0.957
Residuals	160	35.075		

Table 4B Multiple comparisons of tissue elastic moduli

Tissue	**emmean**	**SE**	**df**	**lower.CL**	**upper.CL**	**Group**
Bundle	0.4997	0.0639	160	0.3734	0.6259	**a**
Pith	1.0069	0.0611	160	0.8861	1.1277	**b**
Rind	2.1989	0.0611	160	2.0781	2.3197	**c**

Acknowledgments This research was sponsored by the National Science Foundation under grant CMMI-1761015.

Declarations

Conflict of Interests The authors declare that they have no conflict of interest.

References

1. Chitnis P (2020) NIFA Recent Changes and Future Direction National Association of Plant Breeder 2020 Annual Meeting, Virtual Meeting, August 16–20
2. Chu T et al (2017) Assessing lodging severity over an experimental maize (Zea mays L.) field using UAS images. Remote Sens 9(9):923
3. Zargar O, Pharr M, Muliana A (2022) Modeling and simulation of creep response of sorghum stems: towards an understanding of stem geometrical and material variations. Biosyst Eng 217:1–17
4. Al-Zube L et al (2018) The elastic modulus for maize stems. Plant Methods 14(1):1–12
5. Shah DU, Reynolds TP, Ramage MH (2017) The strength of plants: theory and experimental methods to measure the mechanical properties of stems. J Exp Bot 68(16):4497–4516
6. Buchanan AH (1990) Bending strength of lumber. J Struct Eng 116(5):1213–1229
7. Lindström H, Harris P, Nakada R (2002) Methods for measuring stiffness of young trees. Holz als Roh-und Werkstoff 60(3):165–174
8. Zargar O et al (2022) Thigmostimulation alters anatomical and biomechanical properties of bioenergy sorghum stems. J Mech Behav Biomed Mater 127:105090
9. Bashford L et al (1976) Mechanical properties affecting lodging of sorghum. Trans ASAE 19(5):962–0966
10. Lee S et al (2020) Time-dependent mechanical behavior of sweet sorghum stems. J Mech Behav Biomed Mater 106:103731
11. Esehaghbeygi A et al (2009) Bending and shearing properties of wheat stem of alvand variety. World Appl Sci J 6(8):1028–1032
12. Robertson DJ, Smith SL, Cook DD (2015) On measuring the bending strength of septate grass stems. Am J Bot 102(1):5–11
13. Kretschmann DE (2008) The influence of juvenile wood content on shear parallel, compression, and tension perpendicular to grain strength and mode I fracture toughness of loblolly pine at various ring orientation
14. Zhang L et al (2016) Tensile properties of maize stalk rind. BioResources 11(3):6151–6161
15. Yu M et al (2014) Mechanical shear and tensile properties of selected biomass stems. Trans ASABE 57(4):1231–1242
16. Varanasi P et al (2012) Mechanical stress analysis as a method to understand the impact of genetically engineered rice and Arabidopsis plants. Ind Biotechnol 8(4):238–244
17. Young S, Clancy P (2001) Compression mechanical properties of wood at temperatures simulating fire conditions. Fire Mater 25(3):83–93
18. Niklas KJ (1997) Relative resistance of hollow, septate internodes to twisting and bending. Ann Botany 80(3):275–287
19. Gomez FE et al (2017) Identifying morphological and mechanical traits associated with stem lodging in bioenergy sorghum (Sorghum bicolor). Bioenergy Res 10(3):635–647
20. Wimmer R et al (1997) Longitudinal hardness and Young's modulus of spruce tracheid secondary walls using nanoindentation technique. Wood Sci Technol 31(2):131–141
21. Gindl W et al (2004) Mechanical properties of spruce wood cell walls by nanoindentation. Appl Phys A 79(8):2069–2073
22. Gindl W, Gupta H (2002) Cell-wall hardness and Young's modulus of melamine-modified spruce wood by nano-indentation. Compos Part A: Appl Sci Manuf 33(8):1141–1145
23. Zou L et al (2009) Nanoscale structural and mechanical characterization of the cell wall of bamboo fibers. Mater Sci Engineering: C 29(4):1375–1379
24. Zickler G, Schöberl T, Paris O (2006) Mechanical properties of pyrolysed wood: a nanoindentation study. Phil Mag 86(10):1373–1386
25. Yu Y et al (2007) Cell-wall mechanical properties of bamboo investigated by in-situ imaging nanoindentation. Wood Fiber Science 39(4):527–535
26. Burgert I, Keplinger T (2013) Plant micro-and nanomechanics: experimental techniques for plant cell-wall analysis. J Exp Bot 64(15):4635–4649
27. Green NH et al (2002) Force sensing and mapping by atomic force microscopy. TRAC Trends Anal Chem 21(1):65–74
28. Butt H-J, Cappella B, Kappl M (2005) Force measurements with the atomic force microscope: technique, interpretation and applications. Surf Sci Rep 59(1–6):1–152
29. Fahlén J, Salmén L (2003) Cross-sectional structure of the secondary wall of wood fibers as affected by processing. J Mater Sci 38(1):119–126
30. Fahlén J, Salmén L (2005) Pore and matrix distribution in the fiber wall revealed by atomic force microscopy and image analysis. Biomacromol 6(1):433–438
31. Yarbrough JM, Himmel ME, Ding S-Y (2009) Plant cell wall characterization using scanning probe microscopy techniques. Biotechnol Biofuels 2(1):1–11
32. Cappella B, Dietler G (1999) Force-distance curves by atomic force microscopy. Surf Sci Rep 34(1–3):1–104
33. Mosca G et al (2017) On the micro-indentation of plant cells in a tissue context. Phys Biol 14(1):015003
34. Wang L et al (2006) Comparison of plant cell turgor pressure measurement by pressure probe and micromanipulation. Biotechnol Lett 28(15):1147–1150
35. Weber A et al (2015) Measuring the mechanical properties of plant cells by combining micro-indentation with osmotic treatments. J Exp Bot 66(11):3229–3241
36. Goudenhooft C et al (2019) The remarkable slenderness of flax plant and pertinent factors affecting its mechanical stability. Biosyst Eng 178:1–8
37. De Langre E (2019) Plant vibrations at all scales: a review. J Exp Bot 70(14):3521–3531
38. Stubbs CJ, Larson R, Cook DD (2020) Mapping spatially distributed material properties in finite element models of plant tissue using computed tomography. Biosyst Eng 200:391–399
39. Zhdanov O et al (2020) A new perspective on mechanical characterisation of Arabidopsis stems through vibration tests. J Mech Behav Biomed Mater 112:104041
40. Schimleck L et al (2019) Non-destructive evaluation techniques and what they tell us about wood property variation. Forests 10(9):728
41. Spatz HC, Speck O (2002) Oscillation frequencies of tapered plant stems. Am J Bot 89(1):1–11
42. Spatz H-C, Theckes B (2013) Oscillation damping in trees. Plant Sci 207:66–71
43. Niklas KJ, Moon FC (1988) Flexural stiffness and modulus of elasticity of flower stalks from Allium sativum as measured by multiple resonance frequency spectra. Am J Bot 75(10):1517–1525
44. Grabianowski M, Manley B, Walker J (2006) Acoustic measurements on standing trees, logs and green lumber. Wood Sci Technol 40(3):205–216
45. Kretschmann D (2010) Mechanical properties of wood; Wood handbook: wood as an engineering material: Chap.

5. Centennial ed. General technical report FPL; GTR-190. Madison, WI: US Dept. of Agriculture, Forest Service, Forest Products Laboratory. 190:5.1–5.46
46. Frampton MJ (2019) Acoustic studies for the non-destructive testing of wood
47. Dahle G, Carpenter A, DeVallance D (2016) Non-destructive measurement of the modulus of elasticity of wood using acoustical stress waves. Arboric Urban For 42:227–233
48. Wagner F et al (1989) Scanning of an Oak Log for Internal defects. For. Prod J 39:11/12-62–64
49. Krähenbühl A et al (2012) Knot detection in x-ray ct images of wood. in International Symposium on Visual Computing. Springer
50. Roussel J-R et al (2014) Automatic knot segmentation in CT images of wet softwood logs using a tangential approach. Computers Electron Agric 104:46–56
51. Boukadida H et al (2012) PithExtract: A robust algorithm for pith detection in computer tomography images of wood–Application to 125 logs from 17 tree species Computers electronics in agriculture. 85:90–98
52. Sepúlveda P, Kline DE, Oja J (2003) Prediction of fiber orientation in Norway spruce logs using an X-ray log scanner: a preliminary study. Wood fiber science 35(3):421–428
53. Sepúlveda P, Oja J, Grönlund A (2002) Predicting spiral grain by computed tomography of Norway spruce. J wood Sci 48(6):479–483
54. Alfieri PV, Correa MV (2018) Analysis of biodeterioration wood estate: use different techniques to obtain images. Matéria, 23
55. Petutschnigg A, Flach M, Katz H (2002) Decay recognition for spruce in CT-images. Holz als Roh-und Werkstoff 60(3):219–223
56. Gomez FE et al (2018) High throughput phenotyping of morpho-anatomical stem properties using X-ray computed tomography in sorghum. Plant Methods 14(1):1–13
57. Al-Zube LA et al (2017) Measuring the compressive modulus of elasticity of pith-filled plant stems. Plant Methods 13(1):1–9
58. Zhang L et al (2017) Mechanical behavior of corn stalk pith: an experimental and modeling study. INMATEH-Agricultural Eng 51(1)
59. Stubbs CJ, Sun W, Cook DD (2019) Measuring the transverse Young's modulus of maize rind and pith tissues. J Biomech 84:113–120
60. Gomez FE, Muliana AH, Rooney WL (2018) Predicting stem strength in diverse bioenergy sorghum genotypes. Crop Sci 58(2):739–751
61. Bakeer B et al (2013) On the characterisation of structure and properties of sorghum stalks. Ain Shams Engineering Journal 4(2):265–271
62. Zargar O et al (2022) Elongating rind and pith tissues of Sweet Sorghum stems show elevated responses to mechanical stimulation. Biochemical Systematics and Ecology, in press
63. Wright CT et al (2005) Biomechanics of wheat/barley straw and corn stover. Appl Biochem Biotechnol 121(1):5–19
64. Reddy N, Yang Y (2007) Preparation and characterization of long natural cellulose fibers from wheat straw. J Agricultural Food Chem 55(21):8570–8575
65. Kronbergs E (2000) Mechanical strength testing of stalk materials and compacting energy evaluation. Industrial Crops Products 11(2–3):211–216
66. Tanguy M, Bourmaud A, Baley C (2016) Plant cell walls to reinforce composite materials: relationship between nanoindentation and tensile modulus. Mater Lett 167:161–164
67. Nogata F, Takahashi H (1995) Intelligent functionally graded material: bamboo. Compos Eng 5(7):743–751
68. Amada S et al (1997) Fiber texture and mechanical graded structure of bamboo. Compos Part B: Eng 28(1–2):13–20
69. Li H, Shen S (2011) The mechanical properties of bamboo and vascular bundles. J Mater Res 26(21):2749–2756
70. Speck T et al (1992) *Mechanische Werte* Allgemeine Biologie Pflanzen Tiere. 244–246
71. Speck O, Speck T (2021) Functional morphology of plants–a key to biomimetic applications. New Phytol 231(3):950–956
72. Wang C, Wang L, Thomas C (2004) Modelling the mechanical properties of single suspension-cultured tomato cells. Ann Botany 93(4):443–453
73. Routier-Kierzkowska A-L et al (2012) Cellular force microscopy for in vivo measurements of plant tissue mechanics. Plant Physiol 158(4):1514–1522
74. Ozdemir OC et al (2012) Investigating the structural properties of corn stover biomass. in ASME International Mechanical Engineering Congress and Exposition. Am Soc Mech Eng
75. Arnould O et al (2017) Better insight into the nano-mechanical properties of flax fibre cell walls. Industrial Crops Products 97:224–228
76. Asgari M et al (2020) Nano-indentation reveals a potential role for gradients of cell wall stiffness in directional movement of the resurrection plant Selaginella lepidophylla. Sci Rep 10(1):1–10
77. Baley C et al (2006) Transverse tensile behaviour of unidirectional plies reinforced with flax fibres. Mater Lett 60(24):2984–2987
78. Wu Y et al (2010) Evaluation of elastic modulus and hardness of crop stalks cell walls by nano-indentation. Bioresour Technol 101(8):2867–2871
79. Jäger A et al (2011) The relation between indentation modulus, microfibril angle, and elastic properties of wood cell walls. Compos Part A: Appl Sci Manuf 42(6):677–685
80. Tze W et al (2007) Nanoindentation of wood cell walls: continuous stiffness and hardness measurements. Compos Part A: Appl Sci Manuf 38(3):945–953
81. Hu S et al (2009) Intravital imaging of amyloid plaques in a transgenic mouse model using optical-resolution photoacoustic microscopy. Opt Lett 34(24):3899–3901
82. Han S et al (2013) In vivo virtual intraoperative surgical photoacoustic microscopy. Appl Phys Lett 103(20):203702
83. Zhao Y et al (2016) Time-resolved photoacoustic measurement for evaluation of viscoelastic properties of biological tissues. Appl Phys Lett 109(20):203702
84. Gao X et al (2017) Photoacoustic eigen-spectrum from light-absorbing microspheres and its application in noncontact elasticity evaluation. Appl Phys Lett 110(5):054101
85. Lou C, Xing D (2010) Photoacoustic measurement of liquid viscosity. Appl Phys Lett 96(21):211102
86. Liu Y, Yuan Z (2016) Multi-spectral photoacoustic elasticity tomography. Biomedical Opt Express 7(9):3323–3334
87. Gao G, Yang S, Xing D (2011) Viscoelasticity imaging of biological tissues with phase-resolved photoacoustic measurement. Opt Lett 36(17):3341–3343
88. Jin D et al (2017) Biomechanical and morphological multi-parameter photoacoustic endoscope for identification of early esophageal disease. Appl Phys Lett 111(10):103703
89. Zhao Y et al (2014) Simultaneous optical absorption and viscoelasticity imaging based on photoacoustic lock-in measurement. Opt Lett 39(9):2565–2568
90. Wang Q et al (2018) Quantitative photoacoustic elasticity and viscosity imaging for cirrhosis detection. Appl Phys Lett 112(21):211902
91. Rüggeberg M, Burgert I, Speck T (2010) Structural and mechanical design of tissue interfaces in the giant reed Arundo donax. J Royal Soc Interface 7(44):499–506
92. Sarvazyan AP et al (1998) Shear wave elasticity imaging: a new ultrasonic technology of medical diagnostics. Ultrasound Med Biol 24:1419–1435

93. Zhou F et al (2019) Multiscale simulation of elastic modulus of rice stem. Biosyst Eng 187:96–113